University of Bristol - Explore Bristol Research
General rights

A diagnostic GDGT signature for the impact of hydrothermal activity on surface deposits at the Southwest Indian Ridge

Anyang Pan [a, b, #], Qunhui Yang [a, *], Huaiyang Zhou [a, *], Fuwu Ji [a], Hu Wang [a], Richard D. Pancost [b]

[a] *State Key Laboratory of Marine Geology, School of Ocean and Earth Science, Tongji University, Siping Rd. 1239, Shanghai 200092, China*
[b] *Organic Geochemistry Unit, School of Chemistry, Cabot Institute, University of Bristol, Cantock's Close, Bristol BS8 1TS, UK*

* Corresponding author. Tel: +86 13918209499
E-mail address: yangqh@tongji.edu.cn (Qunhui Yang), zhouhy@tongji.edu.cn (Huaiyang Zhou)

[#] Present address: *SINOPEC Petroleum Exploration and Production Research Institute, Wuxi Institute of Petroleum Geology, 2060 Lihu Road, Wuxi, Jiangsu 213126, China*

Abstract

The impact of hydrothermal activity on wider ocean geochemistry and microbial ecology remains a topic of much interest. To explore whether hydrothermal microbial signatures are exported to surrounding marine sediments or if such organisms serve as an important source of sedimentary organic matter, we determined the distributions of glycerol dialkyl glycerol tetraether (GDGT) membrane lipids in surficial normal marine sediments, metalliferous sediments and low-temperature hydrothermal deposits at newly discovered hydrothermal fields and adjacent areas at the Southwest Indian Ridge (SWIR). The GDGTs in those samples varied significantly, evidently representing a variable influence of the hydrothermal activity. GDGT compositions of surficial background sediments in SWIR were similar to those commonly observed in marine sediments, dominated by GDGTs associated with marine planktonic archaea and especially GDGT-0 and crenarchaeol. In contrast, the GDGTs of metalliferous sediments strongly impacted by hydrothermal activity and low-temperature hydrothermal deposits were markedly different, characterized by high relative abundances of isoprenoid GDGTs (*i*GDGTs)

bearing multiple rings (yielding a higher ring index), low relative abundances of crenarchaeol, and the presence of glycerol monoalkyl glycerol tetraether lipids (GMGTs; so called 'H-tetraethers') that were absent in the normal marine sediments. Sources for these hydrothermal-specific tetraether lipids likely include methanogens and anaerobic methanotrophic archaea (GDGT-0 and GDGT-1-3, respectively), *Thermoprotei* and *Thermoplasmatales* (elevated GDGT-3-4), and other thermophilic archaea including *Methanobacteriales* (GMGTs). Deposits influenced by low-temperature hydrothermal activity also contained higher abundances of branched GDGTs (*br*GDGTs) typically attributed to soil bacteria. The more distal metalliferous sediments influenced by the neutrally buoyant plume did not contain putative hydrothermal GDGTs, having the same GDGT distribution as the background sediments. This suggests that the neutrally buoyant plume has a limited potential to directly influence the organic matter inputs to surrounding sediments, due to a rapidly waning chemosynthetic microbial contribution relative to normal marine contributions as the plume dispersed and was diluted.

1. Introduction

In 1977, scientists diving in the submersible *Alvin* made a stunning discovery on the bottom of the Galapagos Rift in the eastern Pacific Ocean, where seafloor hydrothermal activity and a novel ecosystem were observed (Corliss et al., 1979). Since then, these discoveries have changed our understanding of Earth and life, and 532 active and 56 inactive submarine hydrothermal vent fields have been discovered (Beaulieu et al., 2013). The vent deposits are known to harbor high-

54   biomass benthic communities with chemosynthetic primary producers and other microbes

55   serving as the foundation of the food web (Govenar, 2012). They can use chemical energy,

56   derived from mixing of reduced chemicals such as CH_4, H_2S, H_2 and metals in hydrothermal

57   fluids with oxygenated seawater. Black smoker hydrothermal vents exude fluids with μM–mM

58   Fe concentrations (Von Damm et al., 1985; Douville et al., 2002), which can be as much as seven

59   orders of magnitude greater than typical deep ocean dissolved Fe of ~0.2–0.8 nM (Klunder et al.,

60   2011; Noble et al., 2012; Hatta et al., 2015). Low concentrations of the micronutrient iron in

61   seawater are known to limit primary production and nitrogen fixation in large regions of the

62   global ocean, but recent research demonstrates that dissolved iron from hydrothermal vents can

63   be transported thousands of kilometers from the venting site, contributing to the marine dissolved

64   iron inventory, especially in the abyssal ocean (Toner et al., 2012; Fitzsimmons et al., 2014). In

65   this and other areas, it remains vital to examine the impact of hydrothermal activity on the wider

66   ocean geochemistry and microbial ecology.

67   Diverse microbiological investigations, often involving culture-independent molecular

68   studies of 16S rRNA but also enrichment and isolation studies, have been used to examine

69   microbial diversity in deep-sea hydrothermal vent systems (e.g. Takai et al., 2001; Kormas et al.,

70   2006; Sogin et al., 2006; Jaeschke et al., 2012; Reeves et al., 2014). However, these approaches

71   have inherent limitations, such as inconsistent DNA recovery, kinetic biases inherent in

72   polymerase chain reaction, and the need to develop sepecific and appropriate primers and probes

73   (Chowdhury and Dick, 2012). Organic geochemical approaches also have limitations but can

74   offer a complementary view on microbial community structures since they do not require the

75   culturing of microorganisms, are quantitative and reproducible, and can integrate a longer time

76   window than nucleic acid based researches (Mrozik et al., 2014). There has been some research

on lipid biomarkers in hydrothermal fluids, sulfides, oxides, hydrothermally heated sediments

and organisms from the Mid-Atlantic Ridge, Arctic Mid-Ocean Ridge, East Pacific Rise,

Guyamas Basin spreading center and other hydrothermal systems (e.g. Schouten et al., 2003;

Phleger et al., 2005; Blumenberg et al., 2012; Hu et al., 2012; Jaeschke et al., 2012; Kellermann

et al., 2012; Méhay et al., 2013; Jaeschke et al., 2014; McCollom et al., 2015), including

investigations of intact polar lipids (IPLs) (Gibson et al., 2013; Reeves et al., 2014), and these

have helped reveal the structure and function of chemosynthetic systems. Since Archaea have

high growth temperatures, up to 121 °C (Kashefi and Lovley, 2003), and are widespread in

hydrothermal systems, there have been increasing investigations of archaeal membrane lipids in

submarine and terrestrial hydrothermal sites in recent years (e.g. Schouten et al., 2003; Pearson

et al., 2004, 2008; Pancost et al., 2005, 2006; Boyd et al., 2011; Kaur et al., 2011, 2015; Jaeschke

et al., 2012; Kellermann et al., 2012; Boyd et al., 2013; Gibson et al., 2013; Lincoln et al., 2013;

Méhay et al., 2013; Jaeschke et al., 2014; Reeves et al., 2014).

Here we survey the glycerol dialkyl (and monoalkyl) glycerol tetraether (GDGT and GMGT)

membrane lipid distributions (Fig. 1) at the Southwest Indian Ridge, an area where little work

has been done using either microbiological or organic geochemical approaches (see below). We

examined a combination of hydrothermal deposits and metalliferous (plume) deposits, and used

these to obtain a lipid profile and insights into the archaeal community in the hydrothermal field.

This allowed us to test whether hydrothermal activity impacted the organic matter (OM)

composition of surrounding surface sediments.

2. Samples and methods

2.1. Study area and samples

100   The SWIR is the ultraslow spreading part of the Indian ridge and the sole modern migration

101   pathway between the diverse vent fauna of the Atlantic and Pacific oceans (German et al., 1998;

102   Zhou and Dick, 2013). It is an area of interest, therefore, with respect to the characterization,

103   distribution and migration of submarine microbes, and potentially for the discovery of new deep

104   sea communities (Rogers et al., 2012; Tao et al., 2012; Amon et al., 2015; Chen et al., 2015a,

105   2015b, 2015c, 2015d). Molecular biological (Peng et al., 2011; Li et al., 2013; Li et al, 2015),

106   element geochemistry and mineralogical (Tao et al., 2011, 2012; Cao et al., 2012) studies have

107   been conducted in the SWIR hydrothermal field, but studies of lipid biomarkers and related

108   biogeochemical processes are rare and focused on hydrocarbons and fatty acids in hydrothermal

109   barnacle shells and sulfides (Huang et al., 2014; Lei et al., 2015).

110   The samples described in this paper were recovered from Dragon Vent Field (49°39′ E,

111   37°47′ S), a nearby inactive field (50°28′ E, 37°39.50′ S) and surrounding areas during the

112   DY115-20 and DY115-21 expeditions of R/V Da Yang Yihao in 2009 and 2010 (Fig. 2). Dragon

113   Vent Field, the first active hydrothermal vent to be discovered in the SWIR was found using a

114   remotely operated vehicle from Woods Hole Oceanographic Institution (Tao et al., 2007), at a

115   depth of 2760 m. It harbors many active and inactive sulfide chimneys with mussels, barnacles,

116   sea cucumbers and gastropods (Copley, 2011; Rogers et al., 2012; Tao et al., 2012; Cole et al.,

117   2014). Abundant bivalve and gastropod shells were also observed at the inactive field (~ 200 ×

118   125 m in extent, approximately 73 km away from Dragon Vent Field, at a depth of 1770 m) (Tao

119   et al., 2012).

120   All samples were collected by television grab and divided into three categories (see

121   Supporting Information Table S1) according to the results of mineral and element geochemistry

122   (Pan, 2015): (1) background sediments containing abundant foraminifera detritus, apparently

123 uninfluenced by hydrothermal activity; (2) three metalliferous sediments influenced by various

124 degrees of hydrothermal activity depending on the distance from the hydrothermal vent; and (3)

125 low-temperature hydrothermal deposits enriched in Fe and/or Si, noting that even though these

126 are 'low-temperature' hydrothermal deposits, precipitation temperatures are greater than

127 background sediments of SWIR, ranging between 38.3 to 81.8 °C based on the deduction of

128 oxygen isotopic compositions of amorphous silica in low-temperature hydrothermal deposits

129 from SWIR (Li et al., 2013). Typical samples from the same studied sites (SW35, SW33 and

130 SW36) have been analysed for molecular biology (Peng et al., 2011; Li et al., 2013).

131   The three metalliferous sediments can be classified on the basis of their mineral and element

132 compositions. M-T1 sediments, the furthest from the hydrothermal field, with neutrally buoyant

133 plume fall-outs mixed in, have abundant calcite and slightly higher contents of Fe, Cu and Zn

134 than background sediments. M-T2 sediments, with some oxides mixed in, mainly nontronite and

135 two-line-ferrihydrite, have relatively higher contents of Fe, Mn, Cu and Zn than M-T1, mainly

136 impacting by low-temperature hydrothermal activity. M-T3 sediments have highest Cu and Zn

137 contents, and abundant goethite, representing a direct influence from high-temperature

138 hydrothermal activity (Dias et al., 2008).

139

140 *2.2. Bulk organic parameters*

141   Total carbon (TC) and inorganic carbon (IC) were determined using a Carlo Erba EA1108

142 Elemental Analyzer and a modified Coulomat 702 analyzer, respectively. Total organic carbon

143 (TOC) concentrations were determined by the difference between TC and IC. All reported TOC

144 values were the means of duplicate measurements. Carbon isotopic compositions of TOC

145 ($\delta^{13}C_{TOC}$) were obtained after pretreatment with 4 mol/L HCl with a Flash EA 1112 HT-Delta V

146 Advantage (Thermo Company). The $\delta^{13}C_{TOC}$ [‰ Vienna Pee Dee Belemnite, VPDB] error was

147 ±0.2‰.

148

149 *2.3. Lipid analysis*

150 Two methods were used successively to extract and separate fractions in samples of

151 different types. Metalliferous sediments (M-T2 and M-T3) and low-temperature hydrothermal

152 deposits were processed with method 1, using a modified Bligh-Dyer extraction (Bligh and Dyer,

153 1959) and fractionation protocol based on Dickson et al. (2009). After freeze-drying, about 15 g

154 of each sample were solvent extracted with a culture tube using a single-phase mixture

155 comprised of methanol, chloroform, and aqueous 50 mM phosphate buffer water (pH 7.4) in the

156 volume ratio of 2:1:0.8 (6×). The phases were separated by addition of chloroform and buffer

157 water. The organic phase containing the lipids was collected, and activated copper turnings were

158 added to the extracts for 24 hours to remove elemental sulfur. An aliquot of the total extract was

159 separated into three fractions on a silica column. Fractionation was achieved with

160 chloroform:acetic acid (100:1, v:v), acetone and methanol as eluents to recover simple core

161 lipids (CL), glycolipids (GL) and phospholipids (PL), respectively. The CL fraction was

162 subsequently eluted through a silica column with chloroform saturated with ammonium

163 hydroxide and chloroform:acetic acid (100:1, v:v) to separate neutral components and free fatty

164 acids. GDGTs were not detected in neutral components of the CL fraction based on method 1 and

165 it appears that they were eluted in the GL fraction; previous workers have observed similar

166 behavior and it seems that this method is more appropriate for bacterial membrane lipids (Pitcher

167 et al., 2009).

168 Method 2 was used for the background sediments and M-T1. About 15 g sediments were

169 ultrasonically extracted three times with methanol, dichloromethane:methanol (1:1, v:v) and

170 dichloromethane, respectively (Schouten et al., 2002). The total lipid extract was subsequently

171 separated using a fractionation protocol derived from Oba et al. (2006) and Pitcher et al. (2009),

172 using a silica column and eluting with hexane:ethyl acetate (3:1, v:v), ethyl acetate and methanol

173 to yield CL, GL and PL fractions, respectively.

174   For both methods, to remove polar head groups, 5% HCl in methanol was added to the GL

175 and PL fractions which were then heated at 100 °C for 3 h, after which the organic phase was

176 extracted with double distilled water and chloroform. Because the CL fraction was eluted in the

177 GL fraction in method 1, we have combined GDGT abundances and distributions in the CL and

178 GL fractions for all samples, and discuss only summed CL+GL distributions in order to make an

179 effective comparison among sediments of different types. We also note that silica gel column

180 chromatography separations used in this study are always associated with significant losses of

181 IPL-GDGTs (Lengger et al., 2012); because this likely differs among methodologies, it is

182 inappropriate to compare concentrations even within the constraints of this study – and certainly

183 with other studies. Therefore, this paper focuses soley the distributions of tetraether lipids and

184 how they differ among sediments of different types. This approach should be robust as several

185 studies have shown that although concentrations are methodologically dependent, tetraether lipid

186 distributions are consistent (e.g. Schouten et al., 2009, 2013a). To test this further, we processed

187 one sample with both methods and distributions of GDGTs and GMGTs were similar

188 (see Supporting Information Table S3).

189   Due to the different methods, we do not discuss the potentially fossil vs living signals (core

190 vs intact polar GDGTs). However, we do note that phospholipid distributions (data shown in

191 Supporting Information Table S4) generally show the same relationships among different

192   sediment types as observed for the combined CL+GL fractions discussed below. This is likely a

193   fruitful avenue of future research.

194   Aliquots of all fractions were analysed by high performance liquid chromatography/

195   atmospheric pressure chemical ionisation-MS (HPLC/APCI-MS, Agilent 1100 series) equipped

196   with an autoinjector and Chemstation software (Agilent) in a modification of the procedure of

197   Hopmans et al. (2000) and then Schouten et al. (2007a). Fractions were dissolved in

198   hexane:isopropanol (99:1, v/v) and filtered through 0.45 μm mesh PTFE. Separation of GDGTs

199   was achieved on an Alltech Prevail Cyano column (2.1 mm i.d. $\times$ 150 mm, 3 μm) maintained at

200   30 °C with a flow rate of 0.2 ml/min. Injection volume was 20 μl. GDGTs were eluted

201   isocratically with 99% hexane and 1% isopropanol for 7 min, followed by a linear gradient to

202   1.3% isopropanol at 30 min, to 1.6% isopropanol at 35 min, then increasing to 10% isopropanol

203   at 36 min and kept for 8 min, finally equilibrating with 1% isopropanol for 13 min before the

204   next injection. After each two analyses, the column was cleaned by back-flushing

205   hexane:isopropanol 99:1 (v:v) for 7 min and then rinsed by a linear gradient from 90:10 (v:v)

206   hexane:isopropanol to 99:1 (v:v) hexane:isopropanol within 14 min and equilibrated with 1%

207   isopropanol at 30 min. Conditions for APCI-MS were as follows: vaporizer temperature 380 °C,

208   drying gas (N_2) flow 6 l/min and temperature 200 °C, capillary temperature 282 °C, corona

209   discharge current 3 μA. GDGTs were detected in selected ion monitoring (SIM) mode and were

210   semi-quantified by an internal synthetic C_{46} tetraether standard, based on the procedure of

211   Huguet et al. (2006) and Schouten et al. (2007a).

212   The branched isoprenoid tetraether (BIT) index, a proxy for terrestrial OM input, was used

213   as defined by Hopmans et al. (2004):

214     $$BIT = \frac{[GDGT-I]+[GDGT-II]+[GDGT-III]}{[GDGT-I]+[GDGT-II]+[GDGT-III]+[Cren]} \tag{1}$$

215   , where numbers refer to individual GDGT structures shown in Figure 1. The methylation of

216   branched tetraether (MBT) and cyclization of branched tetraethers (CBT) ratios were used as

217   defined by Weijers et al. (2007):

218

219
$$MBT = \frac{([GDGT-I]+[GDGT-Ia]+[GDGT-Ib])}{\Sigma[all\ branched\ GDGTs]} \qquad (2)$$

220

221
$$CBT = -\log(([GDGT-Ia]+[GDGT-IIa])/([GDGT-Ia]+[GDGT-IIa])) \qquad (3)$$

222

223   The ring index (RI) was defined based on Pearson et al. (2004):

224
$$RI = \frac{1\times[GDGT-1]+2\times[GDGT-2]+3\times[GDGT-3]+4\times[GDGT-4]}{[GDGT-1]+[GDGT-2]+[GDGT-3]+[GDGT-4]} \qquad (4)$$

225

226   The methane index (MI) was used as defined by Zhang et al. (2011):

227
$$MI = \frac{[GDGT-1]+[GDGT-2]+[GDGT-3]}{[GDGT-1]+[GDGT-2]+[GDGT-3]+[Cren]+[Cren']} \qquad (5)$$

228

229   The tetraether index of tetraethers consisting of 86 carbons (TEX$_{86}$) was used as defined by

230   Schouten et al. (2002):

231
$$TEX_{86} = \frac{[GDGT-2]+[GDGT-3]+[Cren']}{[GDGT-1]+[GDGT-2]+[GDGT-3]+[Cren']} \qquad (6).$$

232

233   **3. Results**

234   *3.1. Total organic carbon and carbon isotopic composition*

235   The TOC contents and $\delta^{13}C_{TOC}$ values varied among the different sediment types

236 (Supporting Information Table S1 and Fig. 3). Background sediments had the highest TOC

237 contents (1.2% average) and relatively heavy $\delta^{13}C_{TOC}$ values (-22.1‰ average). Low-

238 temperature hydrothermal deposits had the lowest TOC contents (0.13% average) and more

239 depleted $\delta^{13}C_{TOC}$ values (-24.8‰ average). In the metalliferous sediments, TOC contents and

240 $\delta^{13}C_{TOC}$ values in M-T1 were similar to the background sediments, whereas those parameters in

241 M-T2 were close to those of the low-temperature hydrothermal deposits. TOC contents were

242 slightly higher in M-T3 than M-T2 and low-temperature hydrothermal deposits, but similar

243 $\delta^{13}C_{TOC}$ values.

244

245 *3.2. Tetraether lipid distributions*

246   GDGTs observed in the SWIR samples include a range of isoprenoidal GDGTs (*i*GDGTs)

247 bearing 0 to 4 cyclopentyl moieties as well as crenarchaeol and its regioisomer; a suite of the

248 unusual "H-shaped" glycerol monoalkyl glycerol tetraethers (GMGTs, up to four cyclopentyl

249 moieties but mainly GMGT-0); and surprisingly, branched GDGTs, often in high abundances

250 (*br*GDGTs, including GDGT III-IIIb, GDGT II-IIb, GDGT I-Ib). Trace amounts of glycerol

251 trialkyl glycerol tetraether (GTGT-0; i.e. with one biphytanyl and two phytanyl components and

252 no cyclopentyl moities) were also detected in the low-temperature hydrothermal deposits

253 (Supporting Information Table S2).

254   Among the *i*GDGTs, GDGT-0 and crenarchaeol were dominant in background sediments

255 and M-T1, with crenarchaeol percentages typically being 40-50%. Proportions of GDGTs 1-3

256 were lower and distributions were overall similar to other marine sediments (Schouten et al.,

257 2013b). The proportion of crenarchaeol was markedly lower in M-T2, M-T3 and low-

258 temperature hydrothermal deposits, largely due to higher proportions of GDGTs 0-3 but also

259   GDGT-4, which was not detected in the background sediments. The *i*GDGT distributions of M-

260   T3 was dominated by GDGT-0 and GDGT-4 (Supporting Information Table S2).

261   The isoprenoidal GMGTs (*i*GMGTs) were not detected in background sediments nor in M-

262   T1, but had high relative abundances in the low-temperature hydrothermal deposits and the

263   metalliferous sediments strongly impacted by hydrothermal activity and close to the

264   hydrothermal vent; in fact *i*GMGTs represent >45% of the total tetraether lipids in M-T3, in

265   which GMGT-0 and GMGT-4 were the main components. The proportions of *i*GMGTs in M-T2

266   and low-temperature hydrothermal deposits were lower, but still higher than those of the other

267   sediments, and dominated by GMGT-0.

268   The proportions and abundances of *br*GDGTs were very low in most background samples,

269   M-T1 and M-T3, but markedly higher in M-T2 and low-temperature hydrothermal deposits

270   (>15%). This yielded higher BIT indices for the latter – 0.24 to 0.69 in M-T2 and hydrothermal

271   deposits compared to <0.10 in the other sediment types (Table 1). GDGT-III, GDGT-II and IIa

272   were dominant compounds in most samples. However, GDGT-I was also predominant in M-T2

273   and low-temperature hydrothermal deposits, such that CBT and MBT indices were larger (Table

274   1).

275   In summary, tetraether lipid distributions were dominated by *i*GDGTs in all three SWIR

276   sample categories (Table 1), but the percentages of *i*GDGTs were relatively lower in M-T2, M-

277   T3 and low-temperature hydrothermal deposits, whereas *i*GMGTs were relatively more abundant.

278   Branched GDGTs were also proportionally more abundant in the low-temperature hydrothermal

279   deposits and M-T2. This results in three main groups, shown in the ternary diagram of *i*GDGTs,

280   *i*GMGTs and *br*GDGTs (Fig. 4): Group 1 comprises background sediments and M-T1; Group 2,

281   characterized by relatively higher percentages of *br*GDGTs, comprises some M-T2 and low-

282 temperature hydrothermal deposits; and Group 3, characterized by relatively higher percentages

283 of iGMGTs, comprises the other M-T2 and low-temperature hydrothermal deposits as well as M-

284 T3.

285

286 **4. Discussion – Variations in Organic Matter Sources**

287   TOC contents in SWIR background sediments were higher than the global average for deep-

288 sea surficial sediments (0.25~0.50%, Premuzic et al., 1982). This could be associated with

289 elevated concentrations of phytoplankton and zooplankton in the study area, which has been

290 identified as an important carbon sequestration region (Froneman et al., 1998; Llido et al., 2005).

291 $\delta^{13}C_{TOC}$ values of most background sediments are in the typical range of marine organic matter

292 (-22‰ to -19‰, Fontugne and Jouanneau, 1987), indicating that organic matter of SWIR

293 background sediments was mainly derived from autochthonous marine organisms. This is also

294 consistent with the presence of lipid biomarkers for phytoplankton (i.e. sterols and alkenones,

295 data not shown). The $\delta^{13}C$ values of the metalliferous sediments (except M-T1) and most of the

296 low-temperature hydrothermal deposits were lower, consistent with relatively low $\delta^{13}C$ values

297 for organic matter in other hydrothermal settings (e.g. Southern Mariana Trough, Kato et al.,

298 2010; Loki's Castle, Jaeschke et al., 2012, 2014; PACMANUS, Reeves et al., 2014); this is

299 typically attributed to the production of ^{13}C-depleted OM by chemosynthetic organisms.

300 Intriguingly M-T1 TOC has a $\delta^{13}C$ value similar to that of background sediments, suggesting that

301 deposition of neutrally buoyant plume material has not imparted an obvious hydrothermal OM

302 signature to the areas far away from the hydrothermal vents.

303   To explore these differences in OM source and microbial ecology further we have examined

304 the tetraether lipids of surface sediments from SWIR. Tetraether lipid distributions differ among

305 the normal marine sediments, metalliferous sediments and the low-temperature hydrothermal

306 deposits. Based on the relative distributions of *i*GDGTs, *i*GMGTs and *br*GDGTs, background

307 sediments but also M-T1 have OM sources typical of deep marine sediments, primarily GDGTs

308 exported from overlying waters (Group 1). M-T2 and M-T3 distributions are similar to low-

309 temperature hydrothermal deposits but can still be divided into two sub-groups: Group 2

310 with >11% *br*GDGTs and Group 3 with >10% *i*GMGTs.

311 Combined with the previous molecular biological analyses of samples from the same

312 studied sites at SWIR (Peng et al., 2011; Li et al., 2013), likely sources of different tetraether

313 lipid classes can be assigned. The GDGT-0/crenarchaeol, MIs and RIs all indicate that the

314 hydrothermal deposits have additional archaeal sources compared with background sediments.

315 Moreover, the percentages of *br*GDGTs and BIT indices, combined with unusual MBT/CBT

316 ratios, appear to reflect in situ bacteria production.

317

318 *4.1. Isoprenoidal GDGTs*

319 The *i*GDGTs in background sediments and M-T1 of SWIR were dominated by GDGT-0 and

320 crenarchaeol and lower contents of *i*GDGTs 1-3.This is similar to distributions in the surficial

321 sediments from other oceans and indicates a major contribution to tetraether membrane lipids

322 from non-thermophilic Thaumarchaeota in the marine environment (Schouten et al., 2002).

323 TEX_{86} values in these samples were also consistent with SWIR sea surface temperatures (SSTs,

324 http://www.ospo.noaa.gov/data/sst/contour/global.c.gif) and global calibrations (Fig. 5a; Kim et

325 al., 2010), suggesting a predominantly allochthonous source of water-column GDGTs, which has

326 been confirmed by recent 16s rRNA analysis (mainly Thaumarchaeota, unpublished data).

327 The compositions of *i*GDGTs in most metalliferous sediments and low-temperature

14

328 hydrothermal deposits, with higher contents of total iGDGTs 0-4 and lower contents of

329 crenarchaeol, were different from background sediments. Some of this could be attributed to the

330 presence of crenarchaeota *Thermoprotei* and euryarchaeota *Thermoplasmatales,* previously

331 documented for some of these samples (Peng et al., 2011; Li et al., 2013) and known sources of

332 iGDGTs 1-4 (reviewed in Pearson and Ingalls, 2013; Schouten et al., 2013b).

333   Additional contributions of non-pelagic archaea to the isoprenoidal GDGT pool can be

334 ascertained by testing expected TEX_{86} indices against the RI. Group 2 and 3 sediments are both

335 associated with high RIs, but RIs are higher for the latter and Group 2 TEX_{86} values are similar

336 (albeit at the high end) of the background sediment range. Therefore, it appears that iGDGTs in

337 Group 3 sediments – and perhaps Group 2 sediments – derive from sources additional to those

338 that dominate normal marine sediments, presumably hydrothermal organisms.

339   Additionally, the iGDGT distributions could primarily reflect the different environmental

340 conditions under which Group 2 and 3 sediments formed. TEX_{86} indices in marine sediments

341 have a positive correlation with sea surface temperatures in overlying waters but generally not

342 with pH (e.g. Schouten et al., 2002; Kim et al., 2008, 2010; Boyd et al., 2011). Other studies

343 have also shown that temperature is an important control on the distribution of archaeal tetraether

344 membrane lipids, with RIs increasing with growth temperature (Pearson et al., 2004; Uda et al.,

345 2004; Elling et al., 2015; Kaur et al., 2015). Similar studies, however, have shown that pH also

346 governs GDGT distributions in thermophilic archaea, with RI increasing as pH decreases in

347 diverse settings (e.g. Boyd et al., 2011, 2013; Wu et al., 2013; Kaur et al., 2015).

348   To date, the highest temperature vent fluid observed in the Dragon vent field is 379 °C

349 (unpublished data). Previous studies showed the $pH_{(in\ situ)}$ of the highest temperature vent fluid (>

350 380 °C) measured in situ with solid-state electrochemical sensors, is slightly acidic (5.1–5.4).

351 However, mixing of seawater with vent fluid results in seawater dominated conditions with

352 attendant pH increases (Ding et al., 2005), such that below 121 °C, the upper temperature limit

353 for life (Kashefi and Lovley, 2003), $pH_{(in\ situ)}$ is usually greater than 6.0, approaching neutrality

354 (Ding et al., 2005). It is unclear if a pH range from about 6 to 8 can explain the large variations

355 in GDGT distributions observed here due to the lack of in situ pH information. Pure culture

356 study of marine planktonic thaumarchaeal isolates demonstrated that pH variations over a range

357 of 7.3 to 7.9 exerted a minor influence on GDGT cyclization, however, pH might influence

358 environmental GDGT distribution indirectly by selecting for specific thaumarchaeal lineages

359 with distinct lipid compositions (Elling et al., 2015). Moreover, pH has been shown to be a

360 control on RIs in other settings, albeit over a larger range. Therefore, the unusual *i*GDGT

361 distributions in Group 2 and especially Group 3 likely reflect a range of ecological but also

362 environmental factors, primarily dictated by temperature but possibly also related to pH

363 variations.

364   Both GDGT-0 and crenarchaeol occur in marine group 1 Crenarchaeota, but only GDGT-0

365 appears to be produced by methanogens (Schouten et al., 2007b). The GDGT-0/crenarchaeol

366 ratio in marine group 1 Crenarchaeota typically varies between 0.2 and 2 (Schouten et al., 2002)

367 and ratios >2 suggest an additional source for GDGT-0 (Blaga et al., 2009). The GDGT-

368 0/crenarchaeol ratios were <2 in background sediments and M-T1 (Group 1), whereas the ratios

369 in some metalliferous sediments and low-temperature hydrothermal deposits (Group 3) were > 2

370 (Fig. 5b). Unlike RIs, greater abundances of GDGT-0 are difficult to ascribe to higher

371 temperatures or lower pH and we instead suggest that this is evidence for an additional source,

372 possibly methanogenic archaea. Abundant methanogens (mainly Methanosarcinale or

373 Methanobacteriales) have been detected in some hydrothermal deposits at the same SWIR sites

16

374 (Peng et al., 2011; Li et al., 2013). However, other archaeal species cannot be excluded as

375 contributors (e.g. Pearson et al., 2013; Schouten et al., 2013b; Villanueva et al., 2014) and we

376 note that Archaeoglobales was also detected in these settings (Peng et al., 2011).

377 The GDGT-0/crenarchaeol ratios were <2 in Group 2, which could suggest a hydrothermal

378 origin for both compounds, and crenarchaeol has been found in both terrigenous (e.g. Pearson et

379 al., 2004; Schouten et al., 2007b; Pitcher et al., 2011) and marine hydrothermal systems (Méhay

380 et al., 2013); alternatively, it is consistent with a smaller hydrothermal overprint of Group 2

381 samples (compared to Group 3), consistent with the lower RIs and TEX$_{86}$ values.

382 GDGT MIs below 0.3 to 0.5 are typical of normal marine sediments, whereas MIs of

383 sediments impacted by additional microbial inputs, including anaerobic methanotrophs, are

384 typically >0.5 (Pancost et al., 2001a; Zhang et al., 2011). The MI of most samples of Groups 1

385 and 2 were < 0.3, with several background sediments in the range of 0.3~0.5; in contrast, the MIs

386 of most Group 3 samples were > 0.6 (Fig. 5b), indicating an additional contribution. As

387 hydrothermal plume samples collected from Dragon Vent Field have higher CH$_4$ contents than

388 background water, by at least one order of magnitude (Wang et al., 2015), it seems likely that

389 archaea involved in methane production and consumption could have contributed to the *i*GDGT

390 signature of Group 3, affecting both MIs and %GDGT-0. However, the elevated MIs can also be

391 explained by environmental impacts on GDGT distributions, as discussed above.

392 To explore these two options, we have examined other biomarker classes. Archaeol has

393 always been found in association with anaerobic methane-oxidising Archaea (Blumenberg et al.,

394 2004) and it was found here (1.6–120 ng/g sediment) and was indeed more abundant in the

395 Group 3 sediments (Pan, 2015). Intriguingly, the samples with high MIs, RIs and GDGT-

396 0/crenarchaeol ratios also contained abundant non-isoprenoidal dialkylglycerol ethers (DAGEs)

397 and *iso*/*anteiso*C$_{15:0}$ and *iso*/*anteiso*C$_{17:0}$ fatty acids (Pan, 2015), potentially derived from

398 sulphate-reducing bacteria (Hinrichs et al., 2000; Pancost et al., 2001b). These could reflect

399 independent bacterial inputs, or organisms syntrophically associated with archaeal

400 methanotrophs. However, many thermophilic bacteria synthesize abundant DAGEs and *iso-* and

401 *anteiso*-branched fatty acids (e.g. Huber et al., 1992; Sturt et al., 2004; Yang et al., 2006;

402 Schubotz et al., 2013; Reeves et al., 2014). Moreover, many Archaea (including methanogens,

403 halophiles, Marine Benthic Group B and Miscellaneous Crenarchaeotic Group) produce archaeol

404 (e.g. Koga and Morii, 2005; Lipp and Hinrichs, 2009). In fact, many of these compounds have

405 been detected in hydrothermal deposits that appear to have no AOM influence (e.g. Bradley et al.,

406 2009; Kaur et al., 2011, 2015). As such, the co-occurrence of these biomarkers with high MIs

407 could be evidence for an AOM influence, but that evidence is weak and other explanations

408 remain possible. Compound-specific stable carbon isotope analysis could resolve these

409 competing hypotheses (e.g. Pancost et al., 2001a; Elvert et al., 2005; Niemann and Elvert, 2008),

410 but that was not possible due to their low abundances.

411

412 *4.2. Isoprenoidal GMGTs*

413   Isoprenoidal GMGTs were only found in some metalliferous sediments and low-

414 temperature hydrothermal deposits from the SWIR, being absent in Group 1 sediments and

415 occurring in relatively low abundances in Group 2 (mainly GMGT-0). Abundances were much

416 higher in Group 3 (especially SW40 in M-T3, enriched in copper and zinc, and strongly

417 influenced by high-temperature hydrothermal activity), and dominated by both GMGT-0 and

418 GMGT-4.

419   GMGTs have been found in many marine sediments, albeit at generally low abundances

420   (Schouten et al., 2008); they appear to be particularly abundant in hydrothermal settings,

421   including Loki's Castle (Jaeschke et al., 2012, 2014), Lost City (Lincoln et al., 2013; Méhay et

422   al., 2013) and PACMANUS deep-sea hydrothermal fields (Reeves et al., 2014). They have been

423   reported in *Methanobacteriales* (*Methanothermus fervidus*, Morii et al., 1998), *Thermococcales*

424   (*T. celer*, *P. horikoshii*, Sugai et al., 2004; Jaeschke et al., 2012), DHVE2-cluster

425   (*Aciduliprofundum boonei*, Reysenbach et al., 2006) and *Desulforococcales* (*Ignisphaera*

426   *aggregans*, Knappy et al., 2011). Because a thermophilic crenarchaeon and *Methanobacteriales*

427   were previously detected in some of these samples (Peng et al., 2011; Li et al., 2013), we

428   speculate that GMGTs (and maybe GTGT-0) in the metalliferous sediments and low-temperature

429   hydrothermal deposits mainly originated from these archaea (Schouten et al., 2013b).

430   Additionally, there is a strong positive correlation between RI and percentages of GMGTs

431   (of total tetraethers) in the metalliferous sediments strongly influenced by hydrothermal activity

432   and low-temperature hydrothermal deposits from the SWIR (Fig. 6). A global synthesis shows

433   that this correlation is generally widespread and somewhat consistent across a range of

434   hydrothermal settings (Fig. 6; data from Jaeschke et al., 2012; Lincoln et al., 2013; Jaeschke et

435   al., 2014; Reeves et al., 2014). Given the strong positive linear relationship between RI and

436   temperature (Elling et al., 2015; Kaur et al., 2015), it seems likely temperature also governs the

437   relative abundances of GMGTs – although again, we cannot entirely preclude a pH control.

438   Regardless of the direct control, it seems clear that %GMGTs also are indicative of hydrothermal

439   input in the SWIR, similar to what has been suggested for Lost City Hydrothermal Field (Lincoln

440   et al., 2013).

441

442   *4.3. Branched GDGTs of Putative Bacterial Origin*

443   At the SWIR, proportions of *br*GDGTs are low (<10%) for most background sediments, M-

444   T1, M-T3 and some low-temperature hydrothermal deposits (mainly Group 1 and 3); similarly,

445   BIT indices were generally less than 0.10. These observations are consistent with those from

446   previous studies of open marine sediments, wherein *br*GDGT generally comprise less than 10%

447   of total GDGTs (Schouten et al., 2013b). Moreover, the low percentages of *br*GDGTs in M-T3,

448   which has been influenced by high-temperature hydrothermal activity, are similar to high-

449   temperature hydrothermal sulfides from other areas (Jaeschke et al., 2012; Reeves et al., 2014).

450   However, higher relative amounts of *br*GDGTs occurred in some background marine sediments

451   (e.g. SW12, SW21) of Group 1, the hydrothermally impacted metalliferous sediments (e.g.

452   SW32) and low-temperature hydrothermal deposits (e.g. SW33, SW36, SW41) of Group 2.

453   Distributions also differed, with GDGT-I being dominant over GDGT-III, GDGT-II and GDGT-

454   IIa in Group 1 and 3 but less so in Group 2; similarly, CBT and MBT indices were relatively

455   higher in Group 2 than in Group 1 and 3.

456   Although *br*GDGTs are mainly considered to be products of heterotrophic anaerobic

457   bacteria in terrigenous soil (Weijers et al., 2009), a thermophile source has been inferred for

458   some terrestrial hot springs (Hedlund et al., 2013; Zhang et al., 2013). Furthermore, it seems

459   likely that the terrigenous contribution to the organic matter in the study area, located at an ocean

460   ridge >2000 km away from the nearest mainland, was minor; this is consistent with minor inputs

461   of Al and Ti (terrigenous indicators) and very low abundances of leaf wax biomarkers (high-

462   molecular-weight fatty acids and alkanols, Pan, 2015). Instead, we suggest that the *br*GDGTs in

463   all samples but especially where proportions exceed 10% derive from in situ bacterial production;

464   this could include Acidobacteria which are abundant in some Group 2 samples (SW33 and SW36;

465   Li et al., 2013). Recent studies have shown that *br*GDGTs are synthesized by bacteria in marine

466   sediments (Peterse et al., 2009; Zhu et al., 2011), hydrothermal systems (Hu et al., 2012; Lincoln

467   et al., 2013) and shelf systems (Sinninghe Damsté, 2016). However, it remains unclear why

468   particularly high proportions are largely restricted to Group 2 sediments in this setting.

469

470   *5. Synthesis*

471   At submarine hydrothermal vents, microorganisms thrive on inorganic energy sources, such

472   as methane, reduced iron and manganese that are abundant in hydrothermal vent fluids

473   (Tagliabue et al., 2010; Breier et al., 2012). These inorganic elements are dispersed more widely

474   by hydrothermal plumes rising hundreds of metres off the seafloor and traveling thousands of

475   kilometres from the vents (Dick and Tebo, 2010; Toner et al., 2012; Fitzsimmons et al., 2014).

476   The abundance of chemosynthetic microorganisms within hydrothermal plumes makes such

477   plumes an important dispersal mechanism and a significant source of organic matter to the deep

478   ocean (McCollum, 2000; Lam et al., 2004, 2008). Moreover, these microorganisms appear to be

479   active in plumes and partially determine the geochemical fate of these hydrothermal inputs

480   (Lilley et al., 1995).

481   Previous work has confirmed that species richness and phylogenetic diversity is typically

482   highest near the vent orifice, with the abundance of chemosynthetic microorganisms decreasing

483   with increasing distance from the vent (Sheik et al., 2015). This is consistent with our analyses.

484   The M-T2 and M-T3 sites, with high Fe, Mn, Cu and Zn contents and in close proximity to the

485   vent, have GDGT distributions similar to those of hydrothermal deposits and distinct from

486   background sediments. Overall, the hydrothermal GDGT signature was consistent with previous

487   work and the expected influence of higher growth temperature, including high Ring Indices,

488   TEX$_{86}$ values and %GMGT. Other features, including high %GDGT-0, appear to be consistent

489 with an active methane cycle in these sites. Crucially, the more distal M-T1 sediments have

490 GDGT distributions largely indistinguishable from background sediments, suggesting a rapidly

491 waning chemosynthetic contribution relative to normal marine contributions as the plume

492 dispersed and was diluted.

493

504

505 **References**

506 Amon, D.J., Copley, J.T., Dahlgren, T.G., Horton, T., Kemp, K.M., Rogers, A.D., Glover, A.G.,

507   2015. Observations of fauna attending wood and bone deployments from two seamounts on

508   the Southwest Indian Ridge. Deep-Sea Research Part II: Topical Studies in Oceanography,

509   http://dx.doi.org/10.1016/j.dsr2.2015.07.003.

510 Beaulieu, S.E., Baker, E.T., German, C.R., Maffei, A., 2013. An authoritative global database for

511   active submarine hydrothermal vent fields. Geochemistry Geophysics Geosystems 14, 4892-

512   4905.

513   Blaga, C.I., Reichart, G.-J., Heiri, O., Sinninghe Damsté, J.S., 2009. Tetraether membrane lipid

514   distributions in water-column particulate matter and sediments: a study of 47 European lakes

515   along a north–south transect. Journal of Paleolimnology 41, 523-540.

516   Bligh, E., Dyer, W., 1959. A rapid method of total lipid extraction and purification. Canadian

517   Journal of Biochemistry and Physiology 37, 911-917.

518   Blumenberg, M., Seifert, R., Reitner, J., Pape, T., Michaelis, W., 2004. Membrane lipid patterns

519   typify distinct anaerobic methanotrophic consortia. Proceedings of the National Academy of

520   Sciences of the United States of America 101: 11111-11116.

521   Blumenberg, M., Seifert, R., Buschmann, B., Kiel, S., Thiel, V., 2012. Biomarkers reveal diverse

522   microbial communities in black smoker sulfides from Turtle Pits (Mid-Atlantic Ridge,

523   Recent) and Yaman Kasy (Russia, Silurian). Geomicrobiology Journal 29, 66-75.

524   Boyd, E.S., Pearson, A., Pi, Y., Li, W.-J., Zhang,Y., He, L., Zhang, C.L., Geesey, G.G.,

525   2011.Temperature and pH controls on glycerol dibiphytanyl glycerol tetraether lipid

526   composition in the hyperthermophilic crenarchaeon Acidilobus sulfurireducens.

527   Extremophiles 15, 59-65.

528   Boyd, E.S., Hamilton, T.L., Wang, J., He, L., Zhang, C.L., 2013. The role of tetraether lipid

529   composition in the adaptation of thermophilic archaea to acidity. Frontiers in Microbiology 4,

530   http://dx.doi.org/10.3389/fmicb.2013.00062.

531   Bradley, A.S., Fredricks, H., Hinrichs, K.-U, Summons, R.E., 2009. Structural diversity of

532   diether lipids in carbonate chimneys at the Lost City Hydrothermal Field. Organic

533   Geochemistry 40, 1169-1178.

534   Breier, J.A., Toner, B.M., Fakra, S.C., Marcus, M.A., White, S.N.,Thurnherr, A.M., German,

535   C.R., 2012. Sulfur, sulfides, oxides and organic matter aggregated in submarine

536   hydrothermal plumes at 9°50′N East Pacific Rise. Geochimica et Cosmochimica Acta 88,

537   216-236.

538   Cao, Z., Cao, H., Tao, C., Li, J., Yu, Z., Shu, L., 2012. Rare earth element geochemistry of

539   hydrothermal deposits from Southwest Indian Ridge. Acta Oceanologica Sinica 31, 62-69.

540   Chen C., Linse, K., Roterman, C.N., Copley, J.T., Rogers, A.D., 2015a. A new genus of large

541   hydrothermal vent-endemic gastropod (Neomphalina: Peltospiridae). Zoological Journal of

542   the Linnean Society 175, 319–335.

543   Chen, C., Copley, J.T., Linse, K., Rogers, A.D., Sigwart, J.D., 2015b.The heart of a dragon: 3D

544   anatomical reconstruction of the 'scaly-foot gastropod' (Mollusca: Gastropoda:

545   Neomphalina) reveals its extraordinary circulatory system. Frontiers in Zoology,

546   http://dx.doi.org/10.1186/s12983-015-0105-1.

547   Chen C., Linse, K., Copley, J.T., Rogers, A.D., 2015c. The 'scaly-foot gastropod': a new genus

548   and species of hydrothermal vent-endemic gastropod (Neomphalina: Peltospiridae) from the

549   Indian Ocean. Journal of Molluscan Studies, http://dx.doi.org/10.1093/mollus/eyv013.

550   Chen C., Copley, J.T., Linse, K., Rogers, A.D., 2015d. Low connectivity between 'scaly-foot

551   gastropod' (Mollusca: Peltospiridae) populations at hydrothermal vents on the Southwest

552   Indian Ridge and the Central Indian Ridge. Organisms Diversity & Evolution 15, 663-670.

553   Chowdhury, T.R., Dick, R.P., 2012. Standardizing methylation method during phospholid fatty

554   acid analysis to profile soil microbial communities. Journal of Microbiological Methods 88,

555   285-291.

556   Cole, C., Coelho, A.V., James, R.H., Connelly, D., Sheehan, D., 2014. Proteomic responses to

557   metal-induced oxidative stress in hydrothermal vent-living mussels, Bathymodiolus sp., on

558 the Southwest Indian Ridge. Marine Environmental Research 96, 29-37.

559 Copley, J.T., 2011. Research cruise JC67, Dragon vent field, SW Indian Ocean, 27–30 November

560 2011. In: RRS James Cook cruise report. British Oceanographic Data Centre. Available from

561 http://www.bodc.ac.uk/data/information_and_inventories/cruise_inventory/report /10593/

562 (last accessed 1 March 2016).

563 Corliss, J.B., Dymond, J., Gordon, L.I., Edmond, J.M., von Herzen, R.P., Ballard, R.D., Green,

564 K., Williams, D., Bainbridge, A., Crane, K., van Andel, T.H., 1979. Submarine thermal

565 springs on the Galapagos Rift. Science 203, 1073-1083.

566 Dias, A., Mills, R., Taylor, R., Ferreira, P., Barriga, F., 2008. Geochemistry of a sediment push-

567 core from the Lucky Strike hydrothermal field, Mid-Atlantic Ridge. Chemical Geology 247,

568 339-351.

569 Dick, G.J., Tebo, B.M., 2010. Microbial diversity and biogeochemistry of the Guaymas Basin

570 deep-sea hydrothermal plume. Environmental Microbiology 12, 1334-1347.

571 Dickson, L., Bull, I.D., Gates, P.J., Evershed, R.P., 2009. A simple modification of a silicic acid

572 lipid fractionation protocol to eliminate free fatty acids from glycolipid and phospholipid

573 fractions. Journal of Microbiological Methods 78, 249-254.

574 Ding, K., Seyfried Jr., W.E., Zhang, Z., Tivey, M.K., Von Damm, K.L., Bradley, A.M., 2005. The

575 in situ pH of hydrothermal fluids at mid-ocean ridges. Earth and Planetary Science Letters

576 237, 167-174.

577 Douville, E., Charlou, J.L., Oelkers, E.H., Bienvenu, P., Jove Colon, C.F., Donval, J.P., Fouquet,

578 Y., Prieur, D., Appriou, P., 2002. The rainbow vent fluids (36°14'N, MAR): The influence of

579 ultramafic rocks and phase separation on trace metal content in Mid-Atlantic Ridge

580 hydrothermal fluids. Chemical Geology 184, 37-48.

581   Elling, F.J., Könneke, M., Mußmann, M., Greve, A., Hinrichs, K.-U., 2015. Influence of

582   temperature, pH, and salinity on membrane lipid composition and TEX$_{86}$ of marine

583   planktonic thaumarchaeal isolates. Geochimica et Cosmochimica Acta 171, 238-255.

584   Elvert, M., Hopmans, E.C., Treude, T., Boetius, A., Suess, E., 2005. Spatial variations of

585   methanotrophic consortia at cold methane seeps: implications from a high-resolution

586   molecular and isotopic approach. Geobiology 3, 195-209.

587   Fitzsimmons, J.N., Boyle, E.A., Jenkins, W.J., 2014. Distal transport of dissolved hydrothermal

588   iron in the deep South Pacific Ocean. Proceedings of the National Academy of Sciences 111,

589   16654-16661.

590   Fontugne, M.R., Jouanneau, J.M., 1987. Modulation of the particulate organic carbon flux to the

591   ocean by a macrotidal estuary evidence from measurements of carbon isotopes in organic

592   matter from the Gironde system. Estuarine, Coastal and Shelf Science 24, 377-387.

593   Froneman, P.W., Pakhomov, E.A., Perissinotto, R., Meaton, V., 1998. Feeding and predation

594   impact of two chaetognath species, Eukrohnia hamata and Sagitta gazellae, in the vicinity of

595   Marion Island (Southern ocean). Marine Biology 131, 95-101.

596   German, C.R., Baker, E.T., Mevel, C., Tamaki, K., the FUJI Science Team, 1998. Hydrothermal

597   activity along the southwest indian ridge. Nature 395, 490-493.

598   Gibson, R.A., van der Meer, M.T., Hopmans, E.C., Reysenbach, A.L., Schouten, S., Sinninghe

599   Damsté, J.S., 2013. Comparison of intact polar lipid with microbial community composition

600   of vent deposits of the Rainbow and Lucky Strike hydrothermal fields. Geobiology 11, 72-85.

601   Govenar, B., 2012. Energy transfer through food webs at hydrothermal vents: Linking the

602   lithosphere to the biosphere. Oceanography 25, 246-255.

603   Hatta, M., Measures, C.I., Wu, J., Roshan, S., Fitzsimmons, J.N., Sedwick, P., Morton, P., 2015.

An overview of dissolved Fe and Mn distributions during the 2010–2011 U.S.

GEOTRACES north Atlantic cruises: GEOTRACES GA03. Deep-Sea Research Part II:

Topical Studies in Oceanography 116, 117-129.

Hedlund B.P., Paraiso, J.J., Williams, A.J., Huang, Q., Wei, Y., Dijkstra, P., Hungate, B.A., Dong,

H., Zhang, C.L., 2013. Wide distribution of autochthonous branched glycerol dialkyl

glycerol tetraethers (bGDGTs) in U.S. Great Basin hot springs. Frontiers in Microbiology 4,

http://dx.doi.org/10.3389/fmicb.2013.00222.

Hinrichs, K.-U., Summons, R.E., Orphan, V.J., Sylva, S.P., Hayes, J.M., 2000. Molecular and

isotopic analysis of anaerobic methane-oxidizing communities in marine sediments. Organic

Geochemistry 31, 1685-1701.

Hopmans, E.C., Schouten, S., Pancost, R.D., van der Meer, M.T.J., Sinninghe Damsté, J.S., 2000.

Analysis of intact tetraether lipids in archaeal cell material and sediments by high

performance liquid chromatography atmospheri pressure chemical ionization mass

spectrometry. Rapid Communications in Mass Spectrometry 14, 585-589.

Hopmans, E.C., Weijers, J.W.H., Schefuβ, E., Herfort, L., Sinninghe Damsté, J.S., 2004. A novel

proxy for terrestrial organic matter in sediments based on branched and isoprenoid tetraether

lipids. Earth and Planetary Science Letters 225, 107-116.

Hu, J., Meyers, P.A., Chen, G., Peng, P., Yang, Q., 2012. Archaeal and bacterial glycerol dialkyl

glycerol tetraethers in sediments from the Eastern Lau Spreading Center, South Pacific

Ocean. Organic Geochemistry 43, 162-167.

Huang, X., Zeng, Z., Chen, S., Yin, X., Wang, X., Zhao, H., Yang, B., Rong, K., Ma, Y., 2014.

Component characteristics of organic matter in hydrothermal barnacle shells from Southwest

Indian Ridge. Acta Oceanologica Sinica 32, 60-67.

627 Huber, R., Wilharm, T., Huber, D., Trincone, A., Burggraf, S., König, H., Reinhard, R.,

628   Rockinger, I., Fricke, H., Stetter, K.O., 1992. *Aquifex pyrophilus* gen. Nov. sp. nov.,

629   represents a novel group of marine hyperthermophilic hydrogen-oxidizing bacteria.

630   Systematic Applied Microbiology 15, 340-351.

631 Huguet, C., Hopmans, E.C., Febo-Ayala, W., Thompson, D.H., Sinninghe Damsté, J.S., Schouten,

632   S., 2006. An improved method to determine the absolute abundance of glycerol dibiphytanyl

633   glycerol tetraether lipids. Organic Geochemistry 37, 1036-1041.

634 Jaeschke, A., Jørgensen, S.L., Bernasconi, S.M., Pedersen, R.B., Thorseth, I.H., Früh-Green, G.L.,

635   2012. Microbial diversity of Loki's Castle black smokers at the Arctic Mid-Ocean Ridge.

636   Geobiology 10, 548-561.

637 Jaeschke, A., Eickmann, B., Lang, S.Q., Bernasconi, S.M., Strauss, H., Früh-Green, G.L., 2014.

638   Biosignatures in chimney structures and sediment from the Loki's Castle low-temperature

639   hydrothermal vent field at the Arctic Mid-Ocean Ridge. Extremophiles 18, 545-560.

640 Kashefi, K., Lovley, D.R., 2003. Extending the Upper Temperature Limit for life. Science 301,

641   934.

642 Kato, S., Takano, Y., Kakegawa, T., Oba, H., Inoue, K., Kobavashi, C., Utsumi, M., Marumo, K.,

643   Kobavashi, K., Ito,Y., Ishibashi, J., Yamagishi, A., 2010. Biogeography and biodiversity in

644   sulfide structures of active and inactive vents at deep-sea hydrothermal fields of Southern

645   Mariana Trough. Applied and Environmental Microbiology 76, 2968-2979.

646 Kaur, G., Mountain, B.W., Hopmans, E.C., Pancost, R.D., 2011. Relationship between lipid

647   distribution and geochemical environment within Champagne Pool, Waiotapu, New Zealand.

648   Organic Geochemistry 42, 1203-1215.

649 Kaur, G., Mountain, B.W., Stott, M.B., Hopmans, E.C., Pancost, R.D., 2015. Temperature and pH

control on lipid composition of silica sinters from diverse hot springs in the Taupo Volcanic

Zone, New Zealand. Extremophiles 19, 327-344.

Kellermann, M.Y., Wegener, G., Elvert, M., Yoshinaga, M.Y., Lin, Y.-S., Holler, T., Mollar, X.P.,

Knittel, K., Hinrichs, K.-U., 2012. Autotrophy as a predominant mode of carbon fixation in

anaerobic methane-oxidizing microbial communities. Proceedings of the National Academy

of Sciences 109, 19321-19326.

Kim, J., Schouten, S., Hopmans, E.C., Donner, B., Sinninghe Damsté, J.S., 2008. Global

sediment core-top calibration of the TEX86 paleothermometer in the ocean. Geochimica et

Cosmochimica Acta 72, 1154-1173.

Kim, J.-H., van der Meer, J., Schouten, S., Helmke, P., Willmott, V., Sangiorgi, F., Koç, N.,

Hopmans, E.C., Sinninghe Damsté, J.S., 2010. New indices and calibrations derived from

the distribution of crenarchaeal isoprenoid tetraether lipids: implications for past sea surface

temperature reconstructions. Geochimica et Cosmochimica Acta 74, 4639-4654.

Klunder, M.B., Laan, P., Middag, R., De Baar, H.J.W., van Ooijen, J.C., 2011. Dissolved iron in

the Southern Ocean (Atlantic sector). Deep-Sea Research Part II: Topical Studies in

Oceanography 58, 2678-2694.

Knappy, C.S., Nunn, C.E., Morgan, H.W., Keely, B.J., 2011. The major lipid cores of the

archaeon Ignisphaera aggregans: implications for the phylogeny and biosynthesis of glycerol

monoalkyl glycerol tetraether isoprenoid lipids. Extremophiles 15, 517-528.

Koga, Y., Morii, H., 2005. Recent advances in structural research on ether lipids from archaea

including comparative and physiological aspects. Bioscience Biotechnology and

Biochemistry 69, 2019-2034.

Kormas, K.A., Tivey, M.K., Von Damm, K., Teske, A., 2006. Bacterial and archaeal phylotypes

673   associated with distinct mineralogical layers of a white smoker spire from a deep-sea

674   hydrothermal vent site (9°N, East Pacific Rise). Environmental Microbiology 8, 909-920.

675   Lam, P., Cowen, J.P., Jones, R.D., 2004. Autotrophic ammonia oxidation in a deep-sea

676   hydrothermal plume. FEMS Microbiology Ecology 47, 191-206.

677   Lam, P., Cowen, J.P., Popp, B.N., Jones, R.D., 2008. Microbial ammonia oxidation and enhanced

678   nitrogen cycling in the Endeavour hydrothermal plume. Geochimica et Cosmochimica Acta

679   72, 2268-2286.

680   Lei, J., Chu, F., Yu, X., Li, X., Tao, C., Ge, Q., 2015. Composition and genesis implications of

681   hydrocarbons in 49.6°E hydrothermal area, Southwest Indian Ocean Ridge. Earth Science

682   Frontiers 22, 281-290.

683   Lengger, S.K., Hopmans, E.C., Sinninghe Damsté, J.S., Schouten, S., 2012. Comparison of

684   extraction and work up techniques for analysis of core and intact polar tetraether lipids from

685   sedimentary environments. Organic Geochemistry 47, 34-40.

686   Li, J., Peng, X., Zhou, H., Li, J., Sun, Z., 2013. Molecular evidence for microorganisms

687   participating in Fe, Mn, and S biogeochemical cycling in two low-temperature hydrothermal

688   fields at the Southwest Indian Ridge. Journal of Geophysical Research: Biogeosciences 118,

689   665-679.

690   Li, J., Zhou, H., Fang, J., Wu, Z., Peng, X., 2015. Microbial Distribution in a Hydrothermal

691   Plume of the Southwest Indian Ridge. Geomicrobiology Journal,

692   http://dx.doi.org/10.1080/01490451.2015.1048393.

693   Lilley, M.D., Feely, R.A., Trefry, J.H., 1995. Chemical and biochemical transformations in

694   hydrothermal plumes. In *Seafloor Hydrothermal Systems: Physical, Chemical, Biological,*

695   *and Geological Interactions*. Humphris, S.E., Zierenberg, R.A., Mullineaux, L.S., and

696   Thomson, R.E.(eds). Washington, DC, USA: American Geophysical Union, pp. 369-391.

697   Lincoln, S.A., Bradley, A.S., Newman, S.A., Summons, R.E., 2013. Archaeal and bacterial

698   glycerol dialkyl glycerol tetraether lipids in chimneys of the Lost City Hydrothermal Field.

699   Organic Geochemistry 60, 45-53.

700   Lipp, J.S., Hinrichs, K.-U., 2009. Structural diversity and fate of intact polar lipids in marine

701   sediments. Geochimica et Cosmochimica Acta 73, 6816-6833.

702   Llido, J., Garçon, V., Lutjeharms, J., Sudre, J., 2005. Event-scale blooms drive enhanced primary

703   productivity at the Subtropical Convergence. Geophysical Research Letters, 32-L15611.

704   Méhay, S., Früh-Green, G.L., Lang, S.Q., Bernasconi, S.M., Brazelton, W.J., Schrenk, M.O.,

705   Schaeffer, P., Adam, P., 2013. Record of archaeal activity at the serpentinite-hosted Lost City

706   Hydrothermal Field. Geobiology 11, 570-592.

707   McCollom, T.M., 2000. Geochemical constraints on primary productivity in submarine

708   hydrothermal vent plumes. Deep Sea Research Part I: Oceanographic Research Papers 47,

709   85-101.

710   McCollom, T.M., Seewald, J.S., German, C.R., 2015. Investigation of extractable organic

711   compounds in deep-sea hydrothermal vent fluids along the Mid-Atlantic Ridge. Geochimica

712   et Cosmochimica Acta 156, 122-144.

713   Morii, H., Eguchi, T., Nishihara, M., Kakinuma, K., König, H., Koga, Y., 1998. A novel ether

714   core lipid with H-shaped C 80-isoprenoid hydrocarbon chain from the hyperthermophilic

715   methanogen Methanothermus fervidus. Biochimica et Biophysica Acta (BBA)-Lipids and

716   Lipid Metabolism 1390, 339-345.

717   Mrozik, A., Nowak, A., Piotrowska-Seget, Z., 2014. Microbial diversity in waters, sediments and

718   microbial mats evaluated using fatty acid-based methods. International Journal of

31

719   Environmental Science and Technology 11, 1487-1496.

720 Niemann, H., Elvert, M., 2008. Diagnostic lipid biomarker and stable carbon isotope signatures

721   of microbial communities mediating the anaerobic oxidation of methane with sulphate.

722   Organic Geochemistry 39, 1668-1677.

723 Noble, A.E., Lamborg, C.H., Ohnemus, D.C., Lam, P.J., Goepfert, T.J., Measures, C.I., Frame,

724   C.H., Casciotti, K.L., DiTullio, G.R., Jennings, J.C., Saito, M.A., 2012. Basin-scale inputs of

725   cobalt, iron, and manganese from the Benguela-Angola front to the South Atlantic Ocean.

726   Limnology and Oceanography 57, 989-1010.

727 Oba, M., Sakata, S., Tsunogai, U., 2006. Polar and neutral isopranyl glycerol ether lipid as

728   biomarkers of archaea in near-surface sediments from the Nankai Trough. Organic

729   Geochemistry 37, 1643-1654.

730 Pan, A., 2015. Research on characteristics of lipid biomarkers in the subseafloor hydrothermal

731   environments and terrestrial hot springs. PhD dissertation of Tongji University.

732 Pancost, R.D., Hopmans, E.C., Sinninghe Damsté, J.S., Medinauth Scientific Party, 2001a.

733   Archaeal lipids in Mediterranean cold seeps: molecular proxies for anaerobic methane

734   oxidation. Geochimica et Cosmochimica Acta 65, 1611-1627.

735 Pancost, R.D., Bouloubassi, I., Aloisi, G., Sinninghe Damsté, J.S., Medinauth Scientific Party,

736   2001b. Three series of non-isoprenoidal dialkyl glycerol diethers in cold-seep carbonate

737   crusts. Organic Geochemistry 32, 695-707.

738 Pancost, R.D., Pressley, S., Coleman, J.M., Benning, L.G., Mountain, B.W., 2005. Lipid

739   biomolecules in silica sinters: indicators of microbial biodiversity. Environmental

740   Microbiology 7, 66-77.

741 Pancost, R.D., Pressley, S., Coleman, J.M., Talbot, H.M., Kelly, S.P., Farrimond, P., Schouten, S.,

742   Benning, L.G., Mountain, B.W., 2006. Composition and implications of diverse lipids in

743   New Zealand Geothermal sinters. Geobiology 4, 71-92.

744   Pearson, A., Huang, Z., Ingalls, A., Romanek, C., Wiegel, J., Freeman, K., Smittenberg, R.,

745   Zhang, C., 2004. Nonmarine crenarchaeol in Nevada hot springs. Applied and

746   Environmental Microbiology 70, 5229-5237.

747   Pearson, A., Pi, Y., Zhao, W., Li, W., Li, Y., Inskeep, W., Perevalova, A., Romanek, C., Li, S.,

748   Zhang, C.L., 2008. Factors controlling the distribution of archaeal tetraethers in terrestrial

749   hot springs. Applied and Environmental Microbiology 74, 3523-3532.

750   Pearson, A., Ingalls, A., 2013. Assessing the use of archaeal lipids as marine environmental

751   proxies. Annual Review of Earth and Planetary Sciences 41, 359-384.

752   Peng, X., Chen, S., Zhou, H., Zhang, L., Wu, Z., Li, J., Li, J., Xu, H., 2011. Diversity of biogenic

753   minerals in low-temperature Si-rich deposits from a newly discovered hydrothermal field on

754   the ultraslow spreading Southwest Indian Ridge. Journal of Geophysical Research 116,

755   G03030. http://dx.doi.org/10.1029/2011JG001691.

756   Peterse, F., Kim, J.-H., Schouten, S., Kristensen, D.K., Koç, N., Sinninghe Damsté, J.S., 2009.

757   Constraints on the application of the MBT/CBT palaeothermometer at high latitude

758   environments (Svalbard, Norway). Organic Geochemistry 40, 692-699.

759   Phleger, C.F., Nelson, M.M., Groce, A.K., Cary, S.C., Coyne, K.J., Nichols, P.D., 2005. Lipid

760   composition of deep-sea hydrothermal vent tubeworm Riftia pachyptila, crabs Munidopsis

761   subsquamosa and Bythograea thermydron, mussels Bathymodiolus sp. and limpets

762   Lepetodrilus spp. Comparative Biochemistry and Physiology Part B: Biochemistry and

763   Molecular Biology 141, 196-210.

764   Pitcher, A., Hopmans, E.C., Schouten, S., Sinninghe Damsté, J.S., 2009. Separation of core and

intact polar archaeal tetraether lipids using silica columns: Insights into living and fossil

biomass contributions. Organic Geochemistry 40, 12-19.

Pitcher, A., Hopmans, E.C., Mosier, A.C., Park, S.-J., Rhee, S.-K., Francis, C.A., Schouten, S.,

Sinninghe Damsté, J.S., 2011. Core and intact polar glycerol dibiphytanyl glycerol tetraether

lipids of ammonia-oxidizing archaea enriched from marine and estuarine sediments. Applied

and Environmental Microbiology 77, 3468-3477.

Premuzic, E., Benkovitz, C.M., Gaffney, J., Walsh, J., 1982. The nature and distribution of

organic matter in the surface sediments of world oceans and seas. Organic Geochemistry 4,

63-72.

Reeves, E.P., Yoshinaga, M.Y., Pjevac, P., Goldenstein, N.I., Peplies, J., Meyerdierks, A., Amann,

R., Bach, W., Hinrichs, K.-U., 2014. Microbial lipids reveal carbon assimilation patterns on

hydrothermal sulfide chimneys. Environmental Microbiology 16, 3515-3532.

Reysenbach, A.-L., Liu, Y., Banta, A.B., Beveridge, T.J., Kirshtein, J.D., Schouten, S., Tivey,

M.K., Von Damm, K.L., Voytek, M.A., 2006. A ubiquitous thermoacidophilic archaeon from

deep-sea hydrothermal vents. Nature 442, 444-447.

Rogers, A.D., Boersch-Supan, P.H., Chen, C., Chivers, A., Copley, J.T., Djurhuus, A., Ferrero,

T.J., Huhnerbach, V., Lamont, P., Marsh, L., Muller, E., Packer, M., Read, J.F., Serpetti, N.,

Shale, D., Staples, D., Taylor, M.A., Webster, C., Woodall, L., 2012. Benthic Biodiversity of

Seamounts in the southwest Indian Ocean. Cruise Report "RRS James Cook" Southern

Indian Ocean Seamounts (IUCN/UNDP/ASCLME/ NERC Cruise 66) 7th November–21st

December.

Schouten, S., Hopmans, E.C., Schefuβ, E., Sinninghe Damsté, J.S., 2002. Distributional

variations in marine crenarchaeotal membrane lipids: a new organic proxy for reconstructing

788   ancient sea water temperatures?. Earth and Planetary Science Letters 204, 265-274.

789   Schouten, S., Wakeham, S.G., Hopmans, E.C., Sinninghe Damsté, J.S., 2003. Biogeochemical

790   evidence that thermophilic archaea mediate the anaerobic oxidation of methane. Applied and

791   Environmental Microbiology 69, 1680-1686.

792   Schouten, S., Huguet, C., Hopmans, E.C., Kienhuis, M.V.M., Sinninghe Damsté, J.S., 2007a.

793   Analytical methodology for TEX86 paleothermometry by high performance liquid

794   chromatography/atmospheric pressure chemical ionization-mass spectrometry. Analytical

795   Chemistry 79, 2940-2943.

796   Schouten, S., van der Meer, M.T., Hopmans, E.C., Rijpstra, W.I., Reysenbach, A.L., Ward, D.M.,

797   Sinninghe Damsté, J.S., 2007b. Archaeal and bacterial glycerol dialkyl glycerol tetraether

798   lipids in hot springs of yellowstone national park. Applied Environmental Microbiology 73,

799   6181-6191.

800   Schouten, S., Baas, M., Hopmans, E.C., Sinninghe Damsté, J.S., 2008. An unusual isoprenoid

801   tetraether lipid in marine and lacustrine sediments. Organic Geochemistry 39, 1033-1038.

802   Schouten, S., Hopmans, E.C., van der Meer, J., Mets, A., Bard, E., Bianchi, T.S., Diefendorf, A.,

803   Escala, M., Freeman, K.H., Furukawa, Y., Huguet, C., Ingalls, A., Ménot-Combes, G.,

804   Nederbragt, A.J., Oba, M., Pearson, A., Pearson, E.J., RosellMelé, A., Schaeffer, P., Shah,

805   S.R., Shanahan, T.M., Smith, R.W., Smittenberg, R., Talbot, H.M., Uchida, M., Van Mooy,

806   B.A.S., Yamamoto, M., Zhang, Z., Sinninghe Damsté, J.S., 2009. An interlaboratory study of

807   TEX86 and BIT analysis using high-performance liquid chromatography mass spectrometry.

808   Geochemistry Geophysics Geosystems 10, Q03012, doi:10.1029/2008GC002221.

809   Schouten, S., Hopmans, E.C., Rosell- Melé, A., Pearson, A., Adam, P., Bauersachs, T., Bard, E.,

810   Bernasconi, S.M., Bianchi, T.S., Brocks, J.J., Carlson, L.T., Castañeda, I.S., Derenne, S.,

Doğrul Selver, A., Dutta, K., Eglinton, T., Fosse, C., Galy, V., Grice, K., Hinrichs, K.-U., Huang, Y., Huguet, A., Huguet, C., Hurley, S., Ingalls, A., Jia, G., Keely, B., Knappy, C., Kondo, M., Krishnan, S., Lincoln, S., Lipp, J., Mangelsdorf, K., Martínez-García, A., Ménot, G., Mets, A., Mollenhauer, G., Ohkouchi, N., Ossebaar, J., Pagani, M., Pancost, R.D., Pearson, E.J., Peterse, F., Reichart, G.-J., Schaeffer, P., Schmitt, G., Schwark, L., Shah, S.R., Smith, R.W., Smittenberg, R.H., Summons, R.E., Takano, Y., Talbot, H.M., Taylor, K.W.R., Tarozo, R., Uchida, M., van Dongen, B.E., Van Mooy, B.A.S., Warren, C., Weijers, J.W.H., Werne, J.P., Woltering, M., Xie, S., Yamamoto, M., Yang, H., Zhang, C., Zhang, Y., Zhao, M., Sinninghe Damsté., 2013a. An interlaboratory study of TEX$_{86}$ and BIT analysis of sediments, extracts, and standard mixtures. Geochemistry Geophysics Geosystems 14, 5263-5285.

Schouten, S., Hopmans, E.C., Sinninghe Damsté, J.S., 2013b. The organic geochemistry of glycerol dialkyl glycerol tetraether lipids: A review. Organic Geochemistry 54, 19-61.

Schubotz, F., Meyer-Dombard, D.R., Bradley, A.S., Fredricks, H.F., Hinrichs, K.-U., Shock, E.L., Summons, R.E., 2013. Spatial and temporal variability of biomarkers and microbial diversity reveal metabolic and community flexibility in Streamer Biofilm Communities in the Lower Geyser Basin, Yellowstone National Park. Geobiology 11, 549-569.

Sheik, C.S., Anantharaman, K., Breier, J.A., Sylvan, J.B., Edwards, K.J., Dick, G., 2015. Spatially resolved sampling reveals dynamic microbial communities in rising hydrothermal plumes across a back-arc basin. International Society for Microbial Ecology Journal 9, 1434-1445.

Sinninghe Damsté, 2016. Spatial heterogeneity of sources of branched tetraethers in shelf systems: The geochemistry of tetraethers in the Berau River delta (Kalimantan, Indonesia). Geochimica et Cosmochimica Acta 186, 13-31.

834 Sogin, M.L., Morrison, H.G., Huber, J.A., Mark Welch, D., Huse, S.M., Neal, P.R., Arrieta, J.M.,

835   Herndl, G.J., 2006. Microbial diversity in the deep sea and the underexplored "rare

836   biosphere". Proceedings of the National Academy of Science of the United States of

837   America 103, 12115-12120.

838 Sturt, H.F., Summons, R.E., Smith, K., Elvert M., Hinrichs, K.-U., 2004. Intact polar membrane

839   lipids in prokaryotes and sediments deciphered by high-performance liquid chromatography/

840   electrospray ionization multistage mass spectrometry – new biomarkers for biogeochemistry

841   and microbial ecology. Rapid Communications in Mass Spectrometry 18, 617-628.

842 Sugai, A., Uda, I., Itoh, Y.H., Itoh, T., 2004. The core lipid composition of the 17 strains of

843   hyperthermophilic archaea, Thermococcales. Journal of Oleo Science 53, 41-44.

844 Tagliabue, A., Bopp, L., Dutay, J.-C., Bowie, A.R., Chever, F., Jean-Baptiste, P., Bucciarelli, E.,

845   Lannuzel, D., Remenyi, T., Sarthou, G., Aumont, O., Gehlen, M., Jeandel, C., 2010.

846   Hydrothermal contribution to the oceanic dissolved iron inventory. Nature Geoscience 3,

847   252-256.

848 Takai, K., Komatsu, T., Inagaki, F., Horikoshi, K., 2001. Distribution of archaea in a black

849   smoker chimney structure. Applied and Environmental Microbiology 67, 3618-3629.

850 Tao, C., Lin, J., Guo, S., Chen, Y., Wu, G., Han, X., German, C., Yoerger, D., Zhu, J., Zhou, N.,

851   2007. The Chinese DY115-19 Cruise: Discovery of the first active hydrothermal vent field at

852   the ultraslow spreading Southwest Indian Ridge. InterRidge News 16, 25-26.

853 Tao, C., Li, H., Huang, W., Han, X., Wu, G., Su, X., Zhou, N., Lin, J., He, Y., Zhou, J., 2011.

854   Mineralogical and geochemical features of sulfide chimneys from the 49°39′ E hydrothermal

855   field on the Southwest Indian Ridge and their geological inferences. Chinese Science

856   Bulletin 56, 2828-2838.

857   Tao, C., Lin, J., Guo, S., Chen, Y.J., Wu, G., Han, X., German, C.R., Yoerger, D.R., Zhou, N., Li,

858   H., Su, X., Zhu, J., 2012. First active hydrothermal vents on an ultraslow-spreading center:

859   Southwest Indian Ridge. Geology 40, 47-50.

860   Toner, B., Marcus, M., Edwards, K., Rouxel, O., German, C., 2012. Measuring the form of iron

861   in hydrothermal plume particles. Oceanography 25, 209-212.

862   Uda, I., Sugai, A., Itoh, Y.H., Itoh, T., 2004. Variation in molecular species of core lipids from the

863   order Thermoplasmales strains depends on the growth temperature. Journal of Oleo Science

864   53, 399-404.

865   Villanueva, L., Sinninghe Damsté, J.S., Schouten, S., 2014. A re-evaluation of the archaeal

866   membrane lipid biosynthetic pathway. Nature Reviews Microbiology 12, 438-448.

867   Von Damm, K.L., Edmond, J.M., Grant, B., Measures, C.I., Walden, B., Weiss, R.F., 1985.

868   Chemistry of submarine hydrothermal solutions at 21°N, East Pacific Rise. Geochimica et

869   Cosmochimica Acta 49, 2197-2220.

870   Wang, H., Zhou, H., Yang, Q., Lilley, M.D., Wu, J., Ji, F., 2015. Development and application of

871   a gas chromatography method for simultaneously measuring H_2 and CH_4 in hydrothermal

872   plume samples. Limnology and Oceanography: Methods 13, 722-730.

873   Weijers, J.W.H., Schouten, S., van Den Donker, J.C., Hopmans, E.C., Sinninghe Damsté, J.S.,

874   2007. Environmental controls on bacterial tetraether membrane lipid distribution in soils.

875   Geochimica et Cosmochimica Acta 71, 703-713.

876   Weijers, J.W.H., Panoto, E., van Bleijswijk, J., Schouten, S., Rijpstra, W.I.C., Balk, M., Stams,

877   A.J.M., Sinninghe Damsté, J.S., 2009. Constraints on the biological source(s) of the orphan

878   branched tetraether membrane lipids. Geomicrobiology Journal 26, 402-414.

879   Wu, W., Zhang, C.L., Wang, H., He, L., Li, W., Dong, H., 2013. Impacts of temperature and pH

880   on the distribution of archaeal lipids in Yunnan hot springs, China. Frontiers in Microbiology

881   4, http://dx.doi.org/10.3389/fmicb.2013.00312.

882 Yang, Y.-L., Yang, F.-L., Jao, S.-C., Chen, M.-Y., Tsay, S.-S., Zou, W., Wu, S.-H., 2006.

883   Structural elucidation of phosphoglycolipids from strains of the bacterial thermophiles

884   *Thermus* and *Meiothermus*. Journal of Lipid Research 47, 1823-1832.

885 Zhang, Y.G., Zhang, C.L., Liu, X.-L., Li, L., Hinrichs, K.-U., Noakes, J.E., 2011. Methane Index:

886   A tetraether archaeal lipid biomarker indicator for detecting the instability of marine gas

887   hydrates. Earth and Planetary Science Letters 307, 525-534.

888 Zhang C.L., Wang, J., Dodsworth, J.A., Williams, A.J., Zhu, C., Hinrichs, K.-U, Zheng, F.,

889   Hedlund, B.P., 2013. In situ production of branched glycerol dialkyl glycerol tetraethers in a

890   great basin hot spring (USA). Frontiers in Microbiology 4, http://dx.doi.org/

891   10.3389/fmicb.2013.00181.

892 Zhou, H., Dick, H.J.B., 2013. Thin crust as evidence for depleted mantle supporting the Marion

893   Rise. Nature 494, 195-200.

894 Zhu, C., Weijers, J.W.H., Wagner, T., Pan, J.M., Chen, J.F., Pancost, R.D., 2011. Sources and

895   distributions of tetraether lipids in surface sediments across a large river-dominated

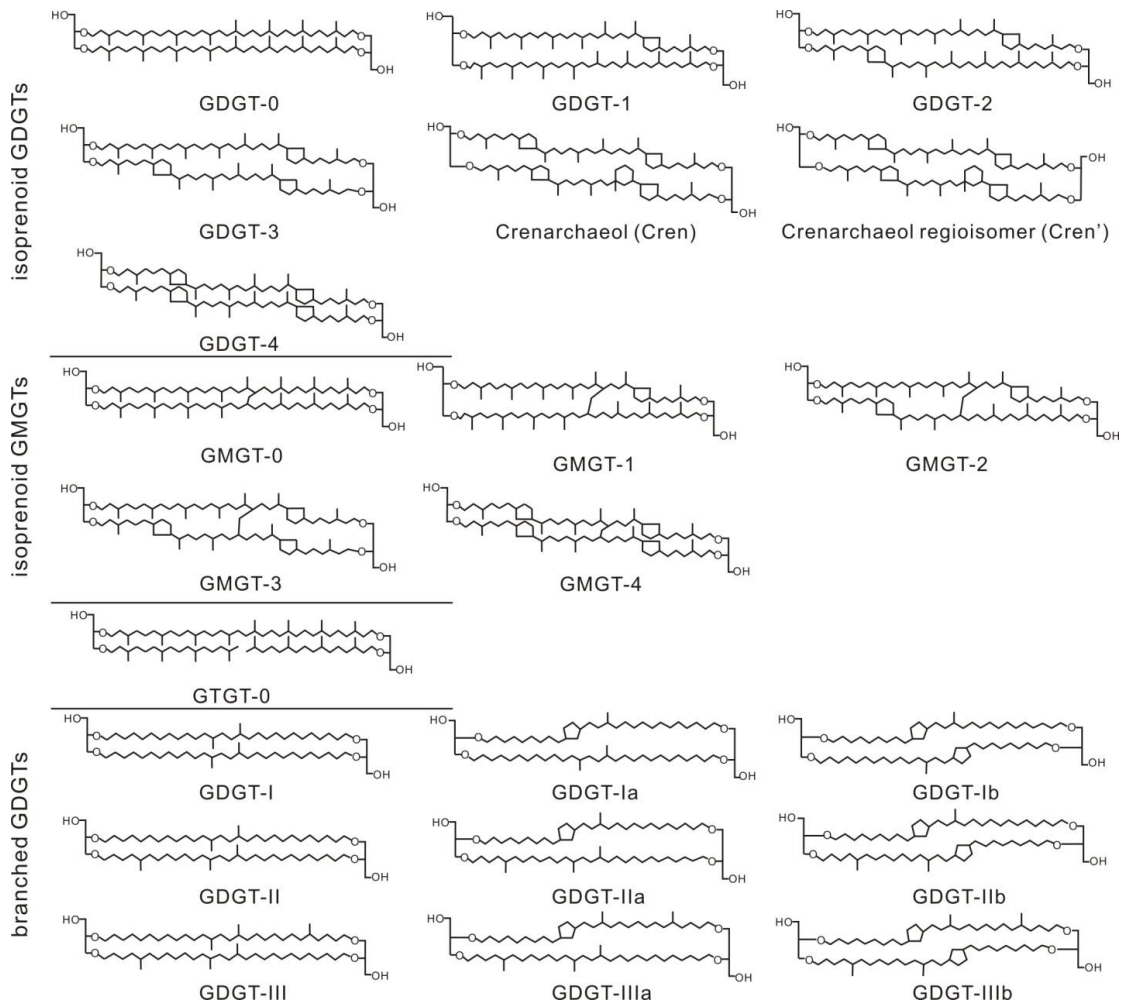896   continental margin. Organic Geochemistry 42, 376-386.

Fig. 1. Structures of tetraether lipids detected in SWIR hydrothermal field.
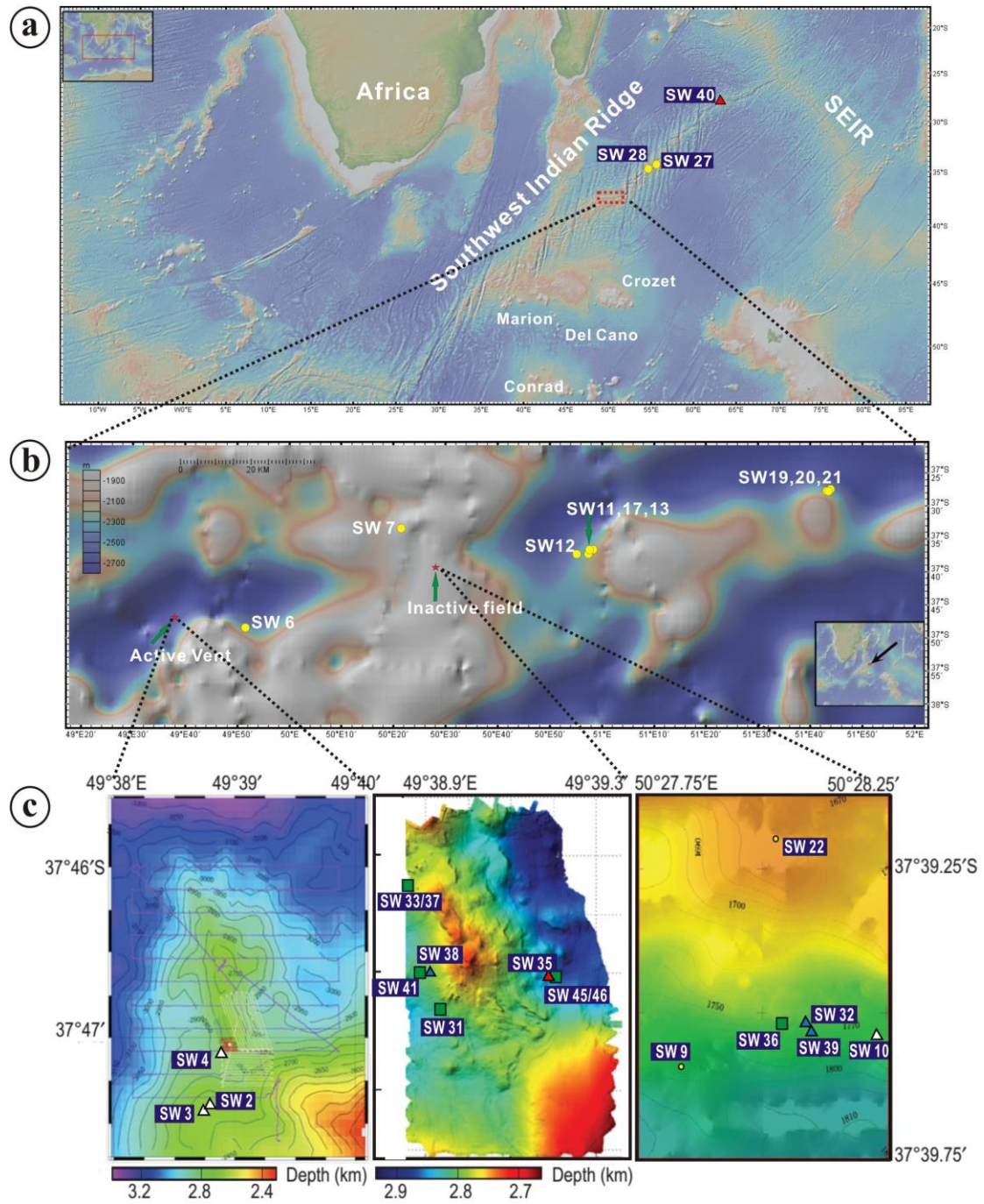
Fig. 2. Location of the samples collected from SWIR. Yellow circles mark background sediments; white, blue and red triangles mark M-T1, M-T2 and M-T3, respectively; green squares mark low-temperature hydrothermal deposits. Panel c modified after (Tao et al., 2012).
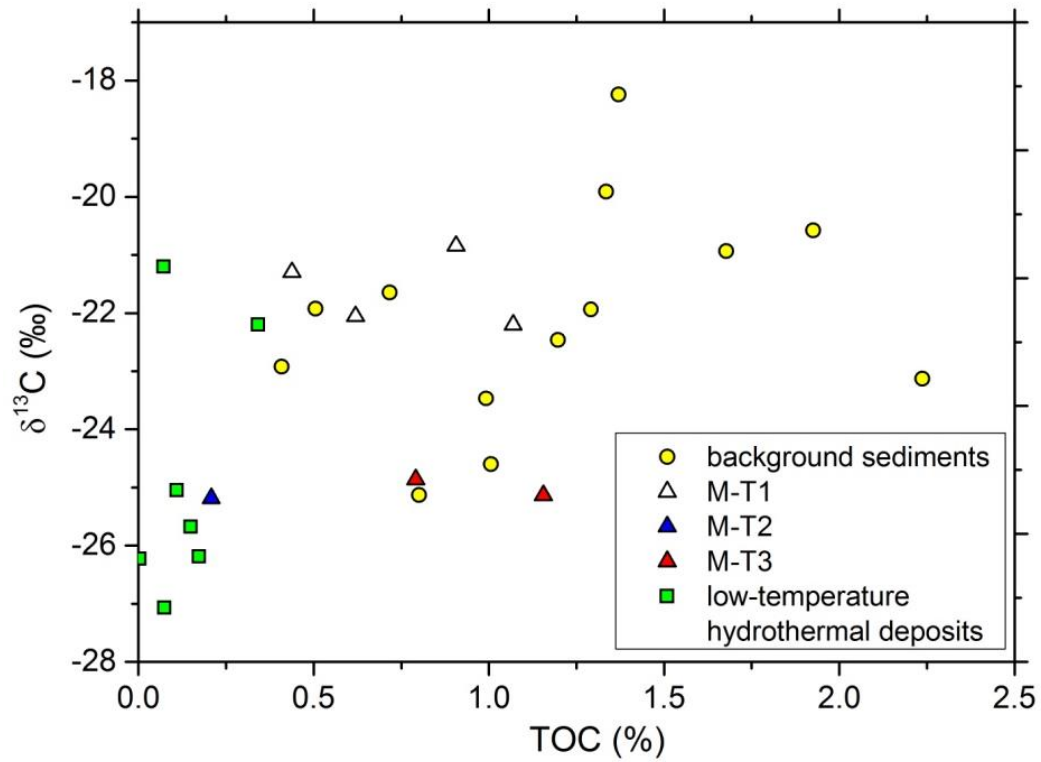
Fig. 3. Crossplot showing the overall positive correlation between TOC content and $\delta^{13}C_{TOC}$ values in background and metalliferous sediments and hydrothermal deposits from the SWIR.
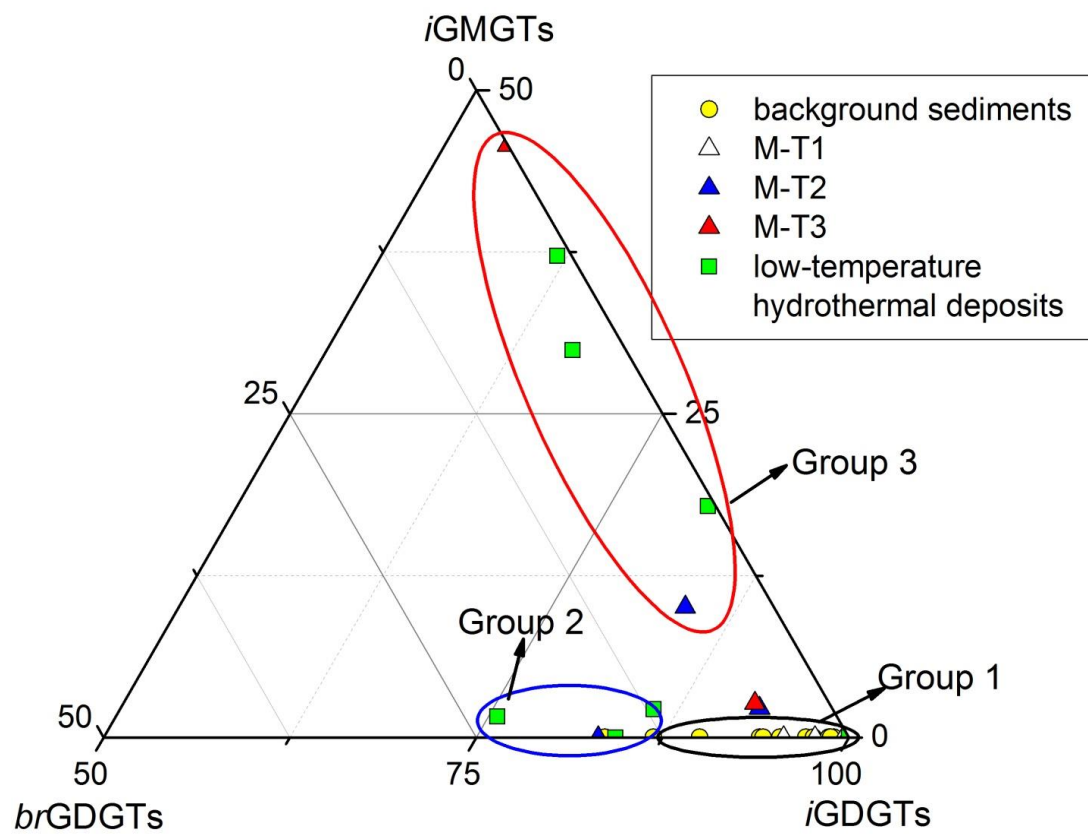
Fig. 4. Ternary diagram of *i*GDGTs, *i*GMGTs and *br*GDGTs in background and metalliferous sediments and hydrothermal deposits from the SWIR. Groups 1 to 3 were divided according to relatively higher contents of *i*GDGTs, *br*GDGTs and *i*GMGTs, respectively.
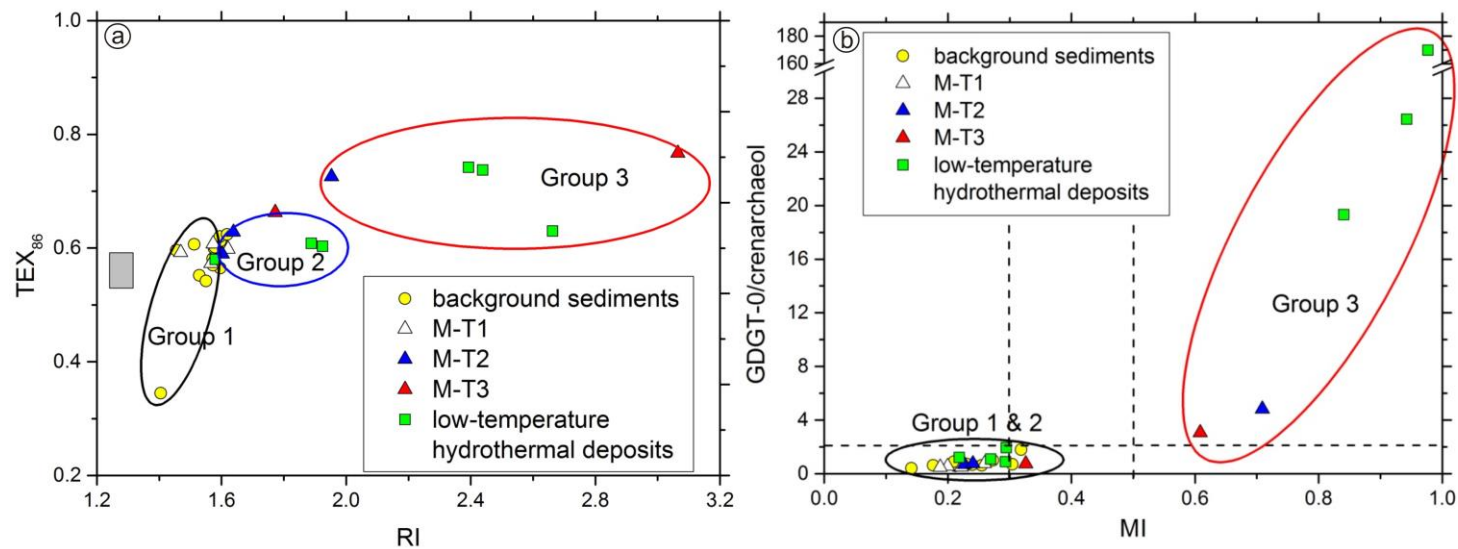
Fig. 5. Crossplots of TEX_{86} versus Ring Index (RI) (Panel a) and MI versus GDGT-0/ crenarchaeol (Panel b) in background and metalliferous

sediments and hydrothermal deposits from the SWIR. In Panel a, the bar shows expected TEX_{86} values for the overlying water sea surface

temperature (SST) of background sediments in the SWIR (SST in the range of 19 to 23 °C according to

http://www.ospo.noaa.gov/data/sst/contour/global.c.gif, and using the TEX_{86}^H calibration of Kim et al., 2010, SST=68.4×logTEX_{86}+38.6); note

that Group 1 but also Group 2 sediments are consistent with this, whereas Group 3 are characterized by higher than expected TEX_{86} values. Both

Group 2 and Group 3 exhibit elevated RIs.
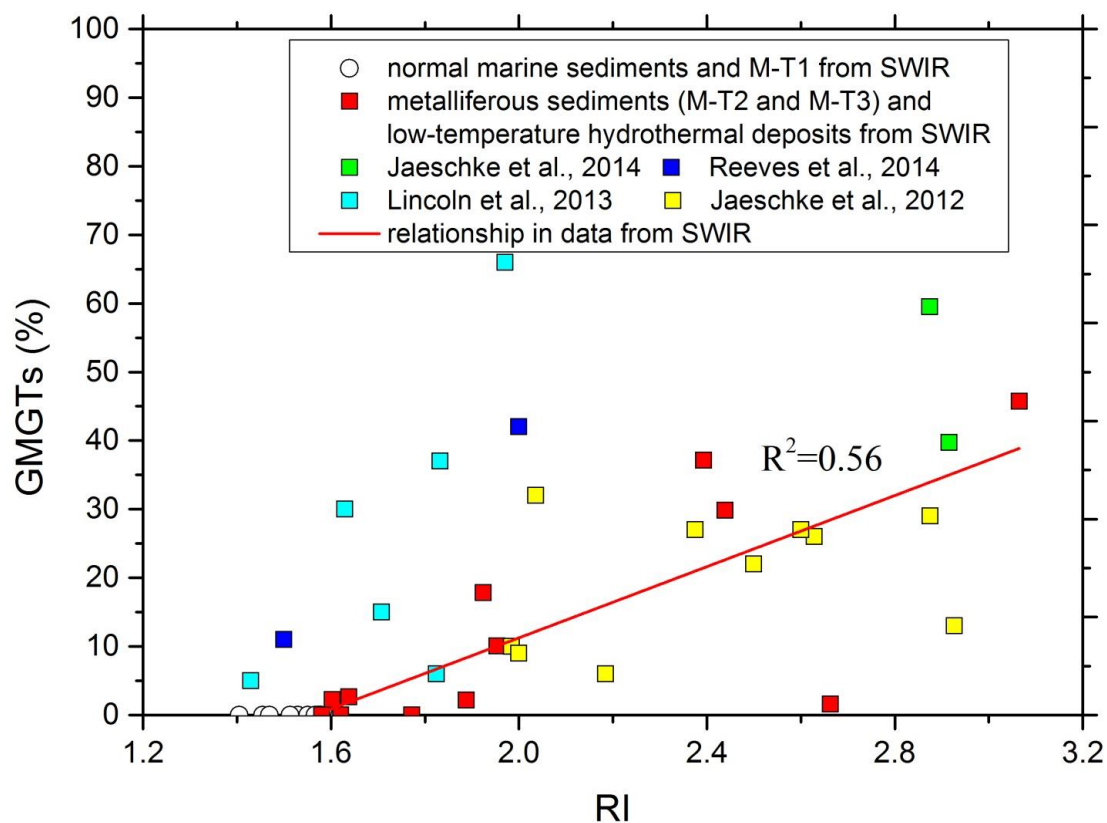
Fig. 6. Crossplot showing %GMGTs (as percentage of total tetraethers) versus RI (ring index) of background and metalliferous sediments and hydrothermal deposits from the SWIR and other hydrothermal systems. The line shows the positive relationship between GMGTs and RI in metalliferous sediments (M-T2 and M-T3) and hydrothermal deposits from SWIR, which is broadly consistent with observations from other sites. Note the several Group 1 and 2 samples with no or low GMGTs and correspondingly low RIs.

Table 1 Various tetraether lipid-based parameters for background sediments, metalliferous sediments and low-temperature hydrothermal deposits from the SWIR.

Type	No.	iGDGTs (%)	iGMGTs (%)	brGDGTs (%)	MBT	CBT	BIT	GDGT-0/ Crenarchaeol	RI	TEX$_{86}$	MI	iGMGTs/ iGDGTs	Group
background sediments	SW6	100	0.00	0.00	—	—	0.00	0.75	1.5	0.55	0.22	0.00	
	SW7	95	0.00	5.0	0.16	-0.11	0.05	0.63	1.6	0.60	0.26	0.00	
	SW9	97	0.00	3.0	0.11	-0.11	0.05	0.71	1.6	0.54	0.30	0.00	
	SW11	99	0.00	1.0	0.00	—	0.02	0.42	1.5	0.61	0.14	0.00	
	SW12	87	0.00	13	0.11	-0.12	0.19	1.0	1.6	0.58	0.27	0.00	
	SW13	98	0.00	2.0	0.09	-0.19	0.03	0.70	1.6	0.61	0.23	0.00	
	SW17	90	0.00	10	0.17	0.17	0.12	0.62	1.5	0.60	0.18	0.00	1
	SW19	99	0.00	1.0	0.13	-0.49	0.01	0.71	1.6	0.56	0.22	0.00	
	SW20	94	0.00	6.0	0.11	0.35	0.10	0.67	1.6	0.61	0.24	0.00	
	SW21	84	0.00	16	0.14	0.14	0.31	1.8	1.4	0.35	0.32	0.00	
	SW22	94	0.00	6.0	0.00	-0.42	0.06	0.59	1.6	0.60	0.21	0.00	
	SW27	99	0.00	1.0	0.27	—	0.03	0.90	1.6	0.57	0.21	0.00	
	SW28	99	0.00	1.0	0.04	0.10	0.02	0.72	1.6	0.62	0.23	0.00	
M-T1	SW2	100	0.00	0.00	0.14	0.44	0.01	0.52	1.6	0.62	0.22	0.00	
	SW3	96	0.00	4.0	0.00	0.12	0.06	0.56	1.5	0.59	0.20	0.00	1
	SW4	98	0.00	2.0	0.00	0.28	0.03	0.50	1.6	0.61	0.19	0.00	
	SW10	100	0.00	0.00	0.00	—	0.00	0.76	1.6	0.57	0.26	0.00	
M-T2	SW32	83	0.00	17	0.44	1.06	0.28	0.71	1.6	0.60	0.23	0.00	2
	SW38	84	10	6.0	0.30	0.12	0.26	4.8	2.0	0.73	0.71	0.12	3
	SW39	93	2.2	4.8	0.28	0.25	0.07	0.76	1.6	0.59	0.24	0.02	n.d.
M-T3	SW35	92	2.7	5.0	0.15	-0.35	0.05	0.75	1.6	0.63	0.33	0.03	n.d.
	SW40	54	46	0.00	—	—	0.00	3.1	3.1	0.77	0.61	0.84	3
low-temperature hydrothermal deposits	SW31	100	0.00	0.00	—	—	0.00	2.0	1.8	0.66	0.29	0.00	n.d.
	SW33	76	1.6	23	0.69	0.04	0.26	0.89	2.7	0.63	0.29	0.02	2
	SW36	84	0.00	16	0.06	-0.28	0.26	1.2	1.6	0.58	0.22	0.00	2
	SW37	82	18	0.52	1.0	—	0.24	26	1.9	0.60	0.94	0.22	3
	SW41	86	2.2	12	0.32	0.83	0.24	1.1	1.9	0.61	0.27	0.03	2
	SW45	66	30	3.6	0.22	0.05	0.42	19	2.4	0.74	0.84	0.45	3
	SW46	62	37	0.94	0.30	0.34	0.69	170	2.4	0.74	0.98	0.60	3

－Some of the components involved in the index were not detected, precluding its calculation.

n.d., not determined; these samples were distinct from Group 1, but not characterized by the defining features of either Group 2 or Group 3.